

Shear partitioning near the central Japan triple junction: the 1923 great Kanto earthquake revisited—II

Fred F. Pollitz,¹ Xavier Le Pichon^{2,3} and Siegfried J. Lallemand²

¹Institute of Theoretical Geophysics, Department of Earth Sciences, University of Cambridge, Downing Street, Cambridge CB2 3EQ, UK

²Laboratoire de Géologie-CNRS URA 1316, Ecole Normale Supérieure, 24 rue Lhomond, 75231, Paris CEDEX 05, France

³Ocean Research Institute, University of Tokyo, 1-15-1 Minamidai, Nakano ku, Tokyo, 164, Japan

Accepted 1996 May 13. Received 1996 May 8; in original form 1995 August 30

SUMMARY

The faulting mechanism of the 1923 great Kanto earthquake is re-examined. The new fault model is constrained by: (1) the focal mechanism of the main shock; (2) triangulation data; (3) levelling data; (4) the distribution of aftershocks; (5) the geology of the ocean floor east of the Boso peninsula; and (6) the delineation of lateral variations in the dip of the subducting Philippine Sea plate. While factors (1)–(4) have been used to constrain earlier fault models, factor (5) leads us to propose the rupture of a major right-lateral fault (here named the Boso transform fault) which accommodated about 1.6 m of slip in the 1923 earthquake. Kinematic constraints derived from the 1923 main-shock fault geometry suggest that the Boso transform fault accommodates about 1.6 cm yr⁻¹ of the relative plate motion, in agreement with onland and marine geology and the uplift history of the Boso peninsula. All plausible fault models of the 1923 earthquake involve right-lateral slip of the Boso transform fault. Triangulation data are better explained by a model which specifies shallower dip of the subducting Philippine Sea slab southeast of the Miura peninsula, consistent with seismological observations.

Key words: earthquakes, fault model, Japan, strike slip, subduction.

1 INTRODUCTION

As one of the most destructive earthquakes in Japanese history, the 1923 September 1, great Kanto earthquake has attracted interest from a number of perspectives. Following the result that the main shock is consistent with the release of accumulated slip roughly perpendicular to the Japan Trench (Kanamori 1971), it was realized that the 1923 earthquake occurred along the Sagami trough and its inland extension (Ando 1971), and that this system is connected with the Nankai trough–Suruga trough as part of the large Philippine Sea plate convergence system (Sugimura 1972). While some studies constrain the fault geometry of the main shock using focal mechanisms, aftershock area, and amplitudes of surface waves (Kanamori & Miyamura 1970; Kanamori 1971), others constrain the total slip using triangulation or levelling data (Ando 1971; Scholtz & Kato 1978; Fujii & Nakane 1983; Matsu'ura & Iwasaki 1983) or tsunami data (Matsuda *et al.* 1978). From a geological point of view, the uplift of the Boso peninsula and Oiso Hill resulting from the 1923 earthquake (e.g. Scholtz & Kato 1978) is correlated with the long-term uplift of these areas (Sugimura & Naruse 1954; Kaneko 1971). Essentially, two different fault geometries have been proposed for the 1923 earthquake. These are illustrated in Fig. 15 of Kanamori (1973), who noted that

the slip as defined by geodetic data is possibly three times larger than that detected by radiated seismic waves. A refinement of these models (Matsuda *et al.* 1978) essentially adopts Ando's (1971) northeast-dipping fault along the Sagami trough, accommodating combined right-lateral and reverse motions, and adds an additional reverse component along a prominent trough at the base of the continental shelf which is kinematically consistent with the sense of slip of the Sagami fault plane. We believe that the key to a better understanding of the rupture process of the 1923 earthquake is to include new constraints provided by the geology of the continental shelf.

Several authors (Yamasaki 1925; Watanabe 1926; Kaine 1967; Kaneko 1972; Research Group for Active Faults of Japan 1991) have pointed out active right-lateral strike-slip faults cutting the Miura and Boso peninsulas that are believed to have been recently active. These ruptures are roughly colinear with topographic scarps of the seafloor extending east of the Boso peninsula. A palinspastic reconstruction (Lallemand *et al.* 1996; hereafter Part I) shows that this lineament is a right-lateral fault extending approximately 150 km from the Miura peninsula through the Boso peninsula and out to sea (Fig. 1) and that it has accommodated approximately 30 km of slip during the Quaternary. Based on these interpretations and the fact that the largest aftershocks following the 1923 main shock

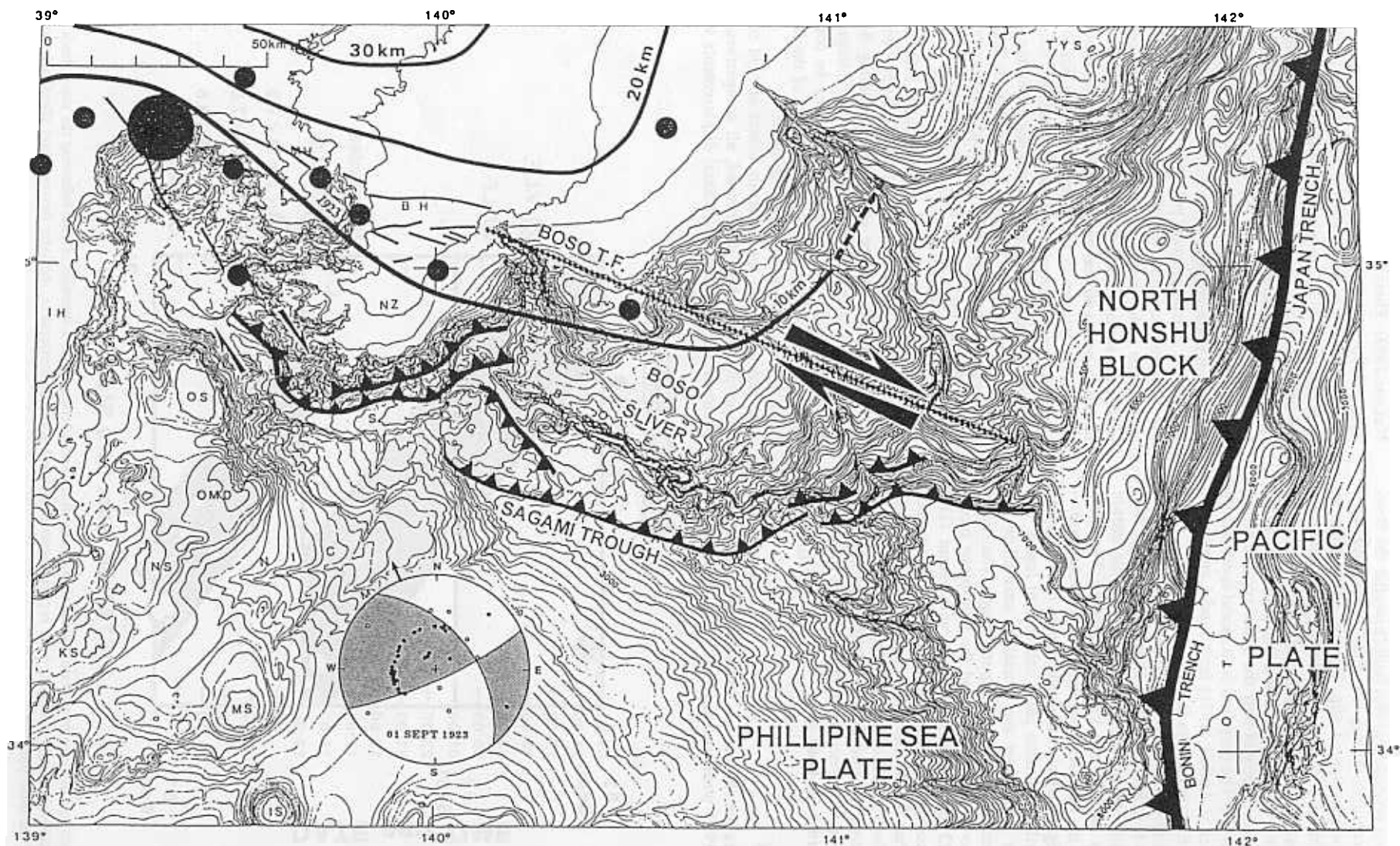


Figure 1. Geological and tectonic setting of the south Kanto district and ocean floor east of the Boso peninsula. Contours in km are those of the Philippine Sea slab after Ishida (1992). Also shown is the redetermined fault-plane solution for the main shock of the 1923 Kanto earthquake using the original first-motion data (Part I). This solution shows that a fault-plane solution consistent with rupture along the Sagami trough is also compatible with the first-motion data.

are possibly located on this fault (Kanamori 1971; Takemura 1994 and Fig. 2), we propose that this fault (hereafter the Boso transform fault) ruptured during the 1923 earthquake with more than 1 m of right-lateral slip. Further refinements to be discussed in this paper involve modelling simultaneously the relevant triangulation and levelling data, and recognizing that the first-motion fault-plane solution (e.g. Kanamori 1971) constrains the fault geometry of only the initial rupture rather than the entire rupture. The proposed fault model is essentially a modified version of Ando's (1971) fault model augmented by slip along the Boso transform fault.

The kinematics of this area have been previously discussed by many authors (e.g. Seno, Stein & Gripp 1993). Both here and in Part I, however, we introduce a new tectonic feature which profoundly modifies the kinematic picture. The Boso transform fault is the northern boundary of a tectonic sliver—the Boso sliver (Fig. 1), which is wedged between the Philippine Sea plate, the northern Honshu plate, and central Japan. The kinematics of the Boso sliver are crucial to unravelling the kinematic relationships around the Sagami trough. The recognition of the Boso transform fault and the fault-plane mechanism of the 1923 main shock, combined with recent GPS results, provide a compelling picture of the long-term kinematics of the region (Part I). In the following sections we shall describe the new fault model of the 1923 sequence, discuss how the faulting sequence fits into the new synthesized kinematic model of the region, and discuss the potential slip release on the faults that border the Boso sliver.

2 DATA SET

Triangulation data for the periods 1880/1902–1924/1926 and 1924/1926–1973/1980 were processed to yield displacement

vectors for the corresponding epochs (Muto 1932; Fujii & Nakane 1983). These are plotted in Figs 3(a)–(b). Three of the displacement vectors closest to the Izu peninsula were taken for the epoch 1931–1973/1980 in order to avoid contamination from the large 1930 Izu earthquake (Matsuda 1972). Five of the triangulation points plotted for the earlier epoch were not obtained for the later epoch (Fig. 6 of Fujii & Nakane 1983); however, the smoothness of the deformation field in the later epoch justifies assigning the displacement of the nearest triangulation point respectively to each of the five missing points. Altogether, 27 triangulation points are used. We aim to obtain the coseismic horizontal deformation field for the 1923 earthquake. The earlier epoch contains this coseismic signal plus a significant signal due to loading of the Philippine Sea plate boundary over a 40 year period. Ignoring post-seismic motions, we take the pattern in the later epoch (Fig. 3b) to represent about 50 years of interseismic strain accumulation. Observational evidence for relatively small post-seismic motions following the 1923 earthquake is given by Scholtz & Kato (1978); physically, the rheology of the crust and upper mantle beneath Kanto district may simply lack a coherent shallow asthenosphere, as is observed in several other areas of Japan (e.g. Thatcher *et al.* 1980; Thatcher 1984; Tabei 1989; Rydelek & Sacks 1990; Pollitz & Sacks 1994), possibly because the complicated convergence of several descending lithospheric slabs inhibits asthenospheric flow. If this interpretation of Fig. 3(b) is accepted, the earlier epoch may be corrected for steady tectonic loading by subtracting 4/5 of the later epoch from it. The result is shown in Fig. 3(c).

In order to avoid the uncertain effects of rigid rotation on the displacement field determined, all comparisons between observed and calculated horizontal displacements were made

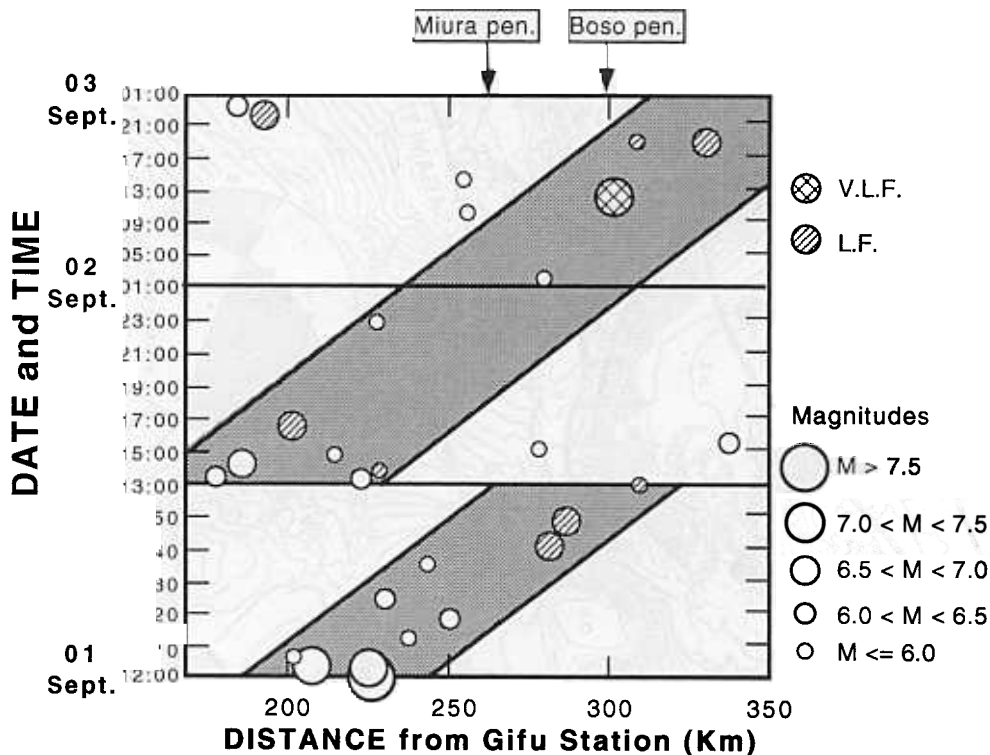


Figure 2. Magnitude and distance from station Gifu of the main shock and aftershocks as a function of time following the main shock (Takemura 1994). Since this station is roughly colinear with rupture areas associated with the earthquake, the later (second day) aftershocks are probably located well east of the Boso peninsula.

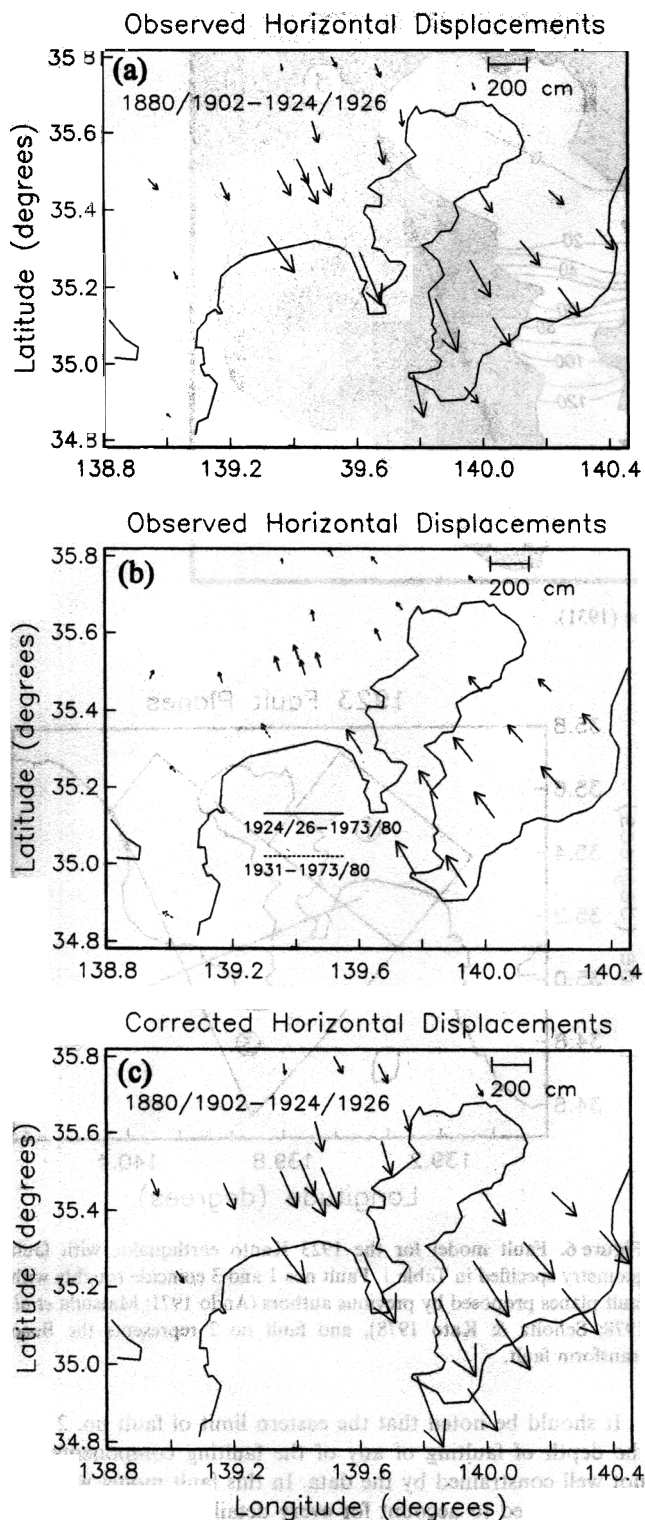


Figure 3. (a) Horizontal displacement vectors for the period 1880/1902–1924/1926 obtained by Muto (1932). (b) Horizontal displacement vectors for the period 1924/1926–1973/1980 or 1931–1973/1980 obtained by Fujii & Nakane (1983). (c) Horizontal displacements from (a) after correction for the effect of steady tectonic loading over a 40 year period, calculated by subtracting 4/5 of (b) from (a). This assumes that (b) represents about 50 years of interseismic strain accumulation. The result in (c) is taken to represent the coseismic horizontal displacements associated with the 1923 earthquake.

by converting the displacement fields into equivalent strain fields. This is done by taking every possible triangle among the triangulation points and evaluating the angle changes associated with the horizontal displacement field. Such a procedure was adopted in Pollitz & Sacks (1994). The misfit between observed and calculated horizontal displacement fields defined by eq. (3) of Pollitz & Sacks (1994) is used in this paper. One triangulation point at 35.47°N, 139.17°E is located very close to the trace of one of the fault planes and was found to be overly sensitive to the parametrization of this fault. For this reason, this triangulation point was omitted from the data set.

The vertical motions in the south Kanto district for the period 1889–1925 are shown in Fig. 4. This figure (Miyabe 1931) is a smoothed version of the levelling results obtained by the Land Survey Department (1928). Two observations are immediately apparent from this figure. First, intense uplift of Oiso Hill and the Miura and Boso peninsulas, and, second, a large depression just to the north of Oiso Hill. The steep decrease of the uplift pattern on the Boso peninsula towards the northeast led Ando (1971) to postulate a 1923 fault rupture in the Sagami trough dipping 45° towards the northeast. Unlike with the triangulation data, the relatively low rate of interseismic uplift of the whole area—of the order of 3 mm yr⁻¹ (Scholtz & Kato 1978)—means that the steady loading component due to 40 years of Philippine Sea plate convergence can be ignored when considering the vertical displacements. As far as the modelling is concerned, it is sufficient to constrain the fault model to fit the two levelling profiles shown in Fig. 5.

3 FAULT MODEL

The fault geometry used in our analysis is shown in Fig. 6, with parameters listed in Table 1. The following observations were taken into account in arriving at this fault geometry.

(1) The main shock occurred on land near Oiso Hill (Kanamori 1971) and evidently propagated towards the south-east. The first-day aftershocks also show a propagation towards the southeast (Fig. 2).

(2) A redetermined fault-plane solution from first arrivals (Part I and Fig. 1) gives the geometry of fault no. 1, which presumably initiated the main shock. The dip of fault no. 1 from the fault-plane solution (42°) is slightly steeper than the local dip of the subducted slab beneath Kanto district (Ishida 1992). To reach a compromise between these two constraints, a dip of 38° is assigned to fault no. 1. Both constraints would be satisfied if the surface of the subducting slab were to become slightly shallower below 10 km depth. The strike of fault no. 1 was chosen to be N39°W following Ando (1971), since this direction is parallel to the strike of the Sagami trough. The redetermined fault-plane solution in Fig. 1 (N42°W) is in very good agreement with this strike.

(3) Large coseismic uplift of the southern Boso peninsula (1.5 m) demands several metres of dip-slip motion on fault no. 3. The triangulation and levelling data are found to be incompatible if the rake of fault no. 3 (λ_3) is taken to be the same as that of fault no. 1. The bathymetry of the Sagami trough (Fig. 1) also supports significant long-term reverse motion along fault no. 3. Therefore, the rake of fault no. 3 is allowed to be variable in order to accommodate a possible greater reverse slip component. The eastern limit of this fault

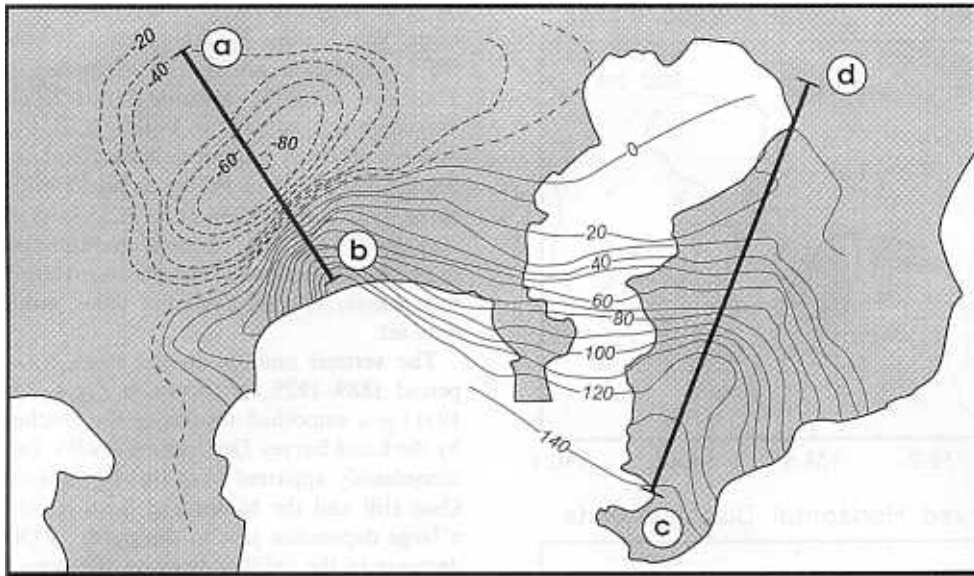


Figure 4. Vertical displacement for the period 1889–1925 obtained by Miyabe (1931).

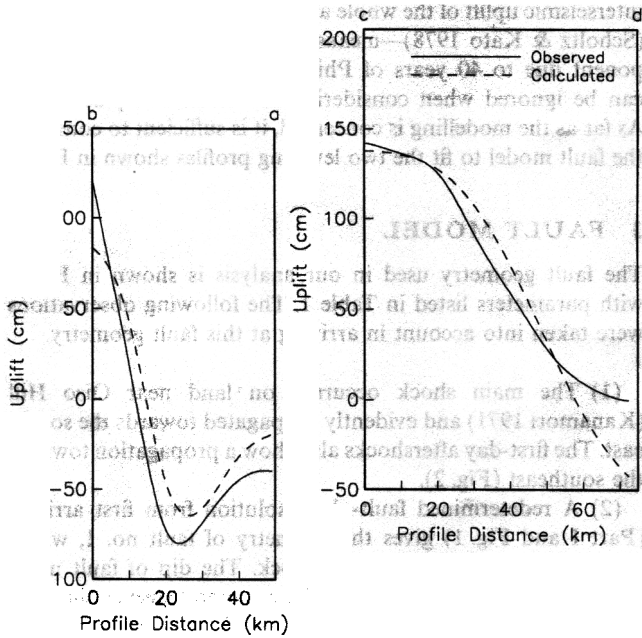


Figure 5. Vertical displacement along profiles a–b and c–d as shown in Fig. 4, plus predicted vertical displacements for the fault model discussed in the text.

is constrained by the lack of a tsunami along the eastern Boso peninsula in 1923, as had occurred previously in 1703 (Matsuda *et al.* 1978).

(4) The dip of fault no. 3 is assigned a value of 20° in order to match the depth to the top of the subducted slab beneath Kanto district (Ishida 1992). The fault must come to the surface along the Sagami trough based on observations discussed by Ando (1971).

(5) Fault no. 2 represents the trace of the active Boso transform fault. Its surface trace is well constrained by the distribution of geologically active faults (e.g. Fig. 1). The dip is taken to be 90° (vertical fault).

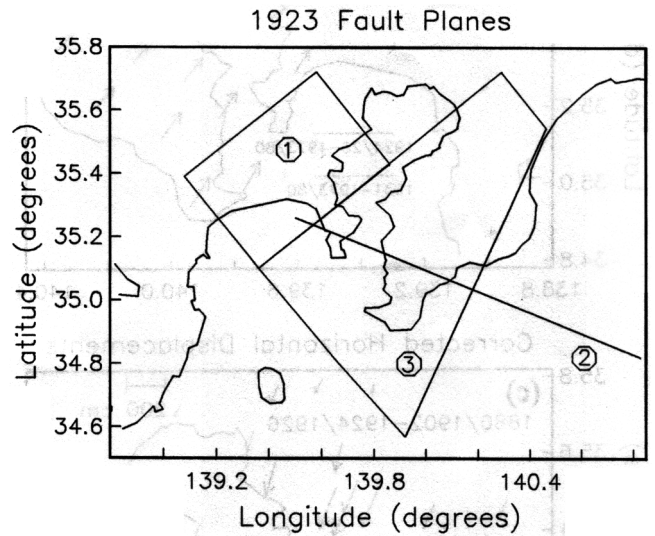


Figure 6. Fault model for the 1923 Kanto earthquake, with fault geometry specified in Table 1. Fault nos 1 and 3 coincide roughly with fault planes proposed by previous authors (Ando 1971; Matsuda *et al.* 1978; Scholtz & Kato 1978), and fault no. 2 represents the Boso transform fault.

It should be noted that the eastern limit of fault no. 2 and the depth of faulting of any of the faulting components are not well constrained by the data. In this fault model we have not attempted to account for every detail in the curvature of the subducted Philippine Sea slab at depth (Ishida 1992, her Fig. 12) because the Philippine Sea slab depth is not well constrained east of the Boso peninsula and the data do not require a more complicated fault model.

The fault slips u_1 , u_2 , u_3 and the rake of fault no. 3 are obtained through a weighted least-squares inversion of the observed horizontal displacements (Fig. 3c) and observed vertical displacements (Fig. 5). Damping is not necessary in order to achieve a reasonable slip distribution. In employing the definition of the misfit in horizontal displacements given

Table 1. 1923 fault model.

segment	strike*	dip (°)	rake**	length (km)	endpoint***		bottom depth (km)	top depth (km)	slip (m)
					lat (°N)	lon (°E)			
1	321	38	156	41	35.39	139.08	46	0.3	u_1
2	292	90	180	130	35.26	139.50	12	0.3	u_2
3'	321	20	λ_3	75	35.12	139.32	40	0.3	u_3

* Degrees clockwise from North.

** Slip direction of hanging wall measured in degrees counterclockwise from strike direction (180° is pure right-lateral strike-slip motion).

*** Uppermost corner of fault closest to strike direction.

' Trapezoidal fault plane.

by eq. (3) of Pollitz & Sacks (1994), we take a constant value for the standard deviation assigned to a constructed angle change. Similarly, we assign a constant value to the standard deviation of an observed uplift datum. By varying the ratio of these constants we can obtain various slip models which fit either the horizontal or vertical displacement data better, with an obvious trade-off between the two fits. Horizontal and vertical displacements for a unit of fault slip at the Earth's surface were obtained by employing the formulas of Okada (1985), taking a shear modulus and bulk modulus of 36 GPa and 65 GPa, respectively. Since Okada's formulas assume a homogeneous half-space, while substantial increases in values of the elastic parameters occur at the lower/upper crust boundary and the Moho, they are only approximations. Errors of up to 25 per cent can occur in calculations involving fault planes extending well into the upper mantle (Yoshioka, Hashimoto & Hirahara 1989), and errors of up to 10 per cent may occur in calculations involving thrust faulting confined to the crust (Pollitz 1996). Since only a fraction of the moment release in our models is below Moho depth, we believe that the assumption of a homogeneous half-space is adequate for the present application.

After choosing values for the weight ratio described above, we inverted for fault slip. The slip values obtained are

$$u_1 = 5.33 \text{ m,}$$

$$u_2 = 1.58 \text{ m,}$$

$$u_3 = 5.06 \text{ m,}$$

$$\lambda_3 = 132.3^\circ.$$

The coseismic horizontal and vertical displacements for these slip models are shown in Figs 7 and 8. Since inversion of the triangulation data set is indeterminate up to a rigid rotation about an arbitrary vertical axis, in comparing the calculated and observed horizontal displacements we find it advantageous to subject the calculated displacements to a 3.5° counterclockwise rotation about the point 36.0°N, 139.9°E. The justification of this procedure is explained in greater detail in Pollitz & Sacks (1994). The rotated calculated displacement vectors are shown in Fig. 9. Overall, the fault model clearly does a good job of fitting both the horizontal displacement data and the levelling data, except around the northern Boso peninsula. A more complicated fault model accounting for the apparent flattening of the subducted Philippine Sea slab beneath the Boso peninsula (Ishida 1992) would probably allow a better fit of this area.

During the process of several inversion trials, we noticed that the slip estimated for fault no. 2 is consistently in the range 1.4–1.8 m, regardless of the relative weights assigned to

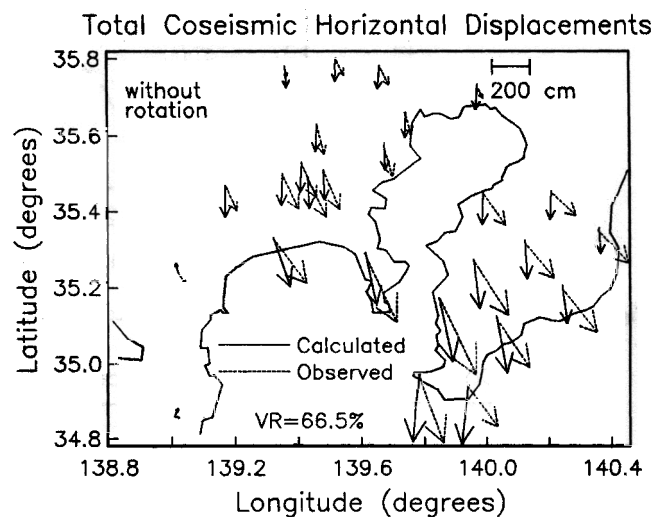


Figure 7. Coseismic horizontal displacements calculated after inverting for fault slip. VR denotes variance reduction with respect to observed horizontal displacements (Fig. 3c), which are also replotted with dotted lines.

the levelling and horizontal displacement data within reasonable limits. This range of slip for fault no. 2 was also obtained in inversions employing the uncorrected horizontal displacement data (Fig. 3a), and the variance reduction with respect to the triangulation data is consistently improved by about 6 per cent by including fault no. 2. For example, assigning zero slip to fault no. 2 and inverting for the slip of faults nos 1 and 3 using the same weight ratio as before yields

$$u_1 = 5.51 \text{ m,}$$

$$u_3 = 4.98 \text{ m,}$$

$$\lambda_3 = 132.9^\circ.$$

The horizontal displacement field calculated from this model is shown in Fig. 10, together with the trace of fault no. 2. Comparing Figs 9 and 10, it is clear that the 6 per cent improvement in variance reduction is due to improved fit of the displacements along the Miura and southern Boso peninsulas. The participation of the Boso transform fault in the 1923 earthquake with about 1.6 m of right-lateral slip is therefore considered a robust result on the basis of the horizontal displacement data.

In the context of our inversion procedure, which employs a fixed weighting of the horizontal and vertical data, we can address more rigorously the question of errors in the slip estimates by performing a simple statistical analysis. Since we

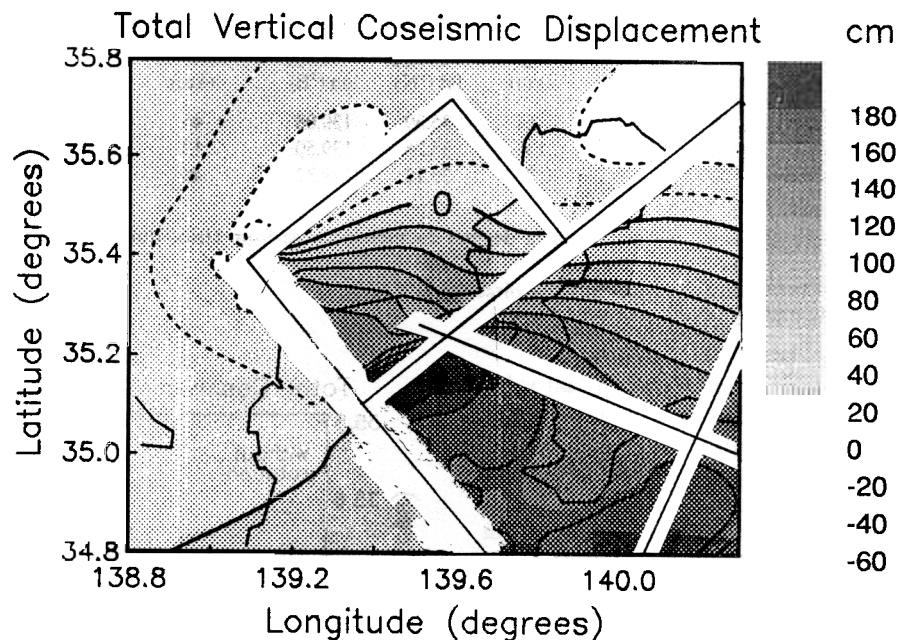


Figure 8. Geographic pattern of coseismic vertical displacements calculated after inverting for fault slip. This can be compared directly with Fig. 4.

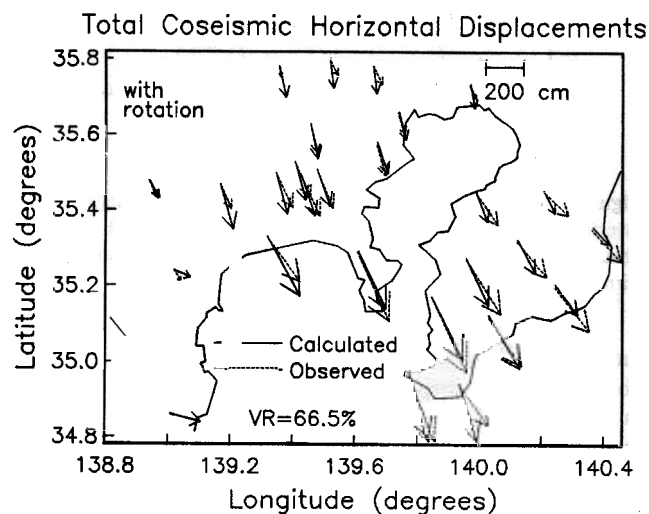


Figure 9. Rotated coseismic horizontal displacements calculated after subjecting the pattern in Fig. 7 to a 3.5° counterclockwise rotation about a vertical axis at 36.0°N , 139.9°E . This rotation was determined visually in order to make a better comparison between the calculated and observed horizontal displacements. Variance reduction is unchanged because misfit is defined in terms of strain, which is invariant with respect to rigid rotation of the displacement field.

do not work with the original triangulation data, but rather with velocity vectors processed from the triangulation data, we address the errors that may occur in the velocity vectors. A typical error in a historic triangulation survey is 1 arcsec, and a typical measuring distance is about 20 km. This yields an error of the order of 10 cm in the position of a given triangulation point. Although position errors are likely to be correlated because they were derived from triangulation data, the worst case (as far as obtaining errors in the slip estimate is concerned) is realized by allowing the position errors to be uncorrelated. Our inversion scheme takes the position vectors, converts them into dimensionless angle changes, then inverts

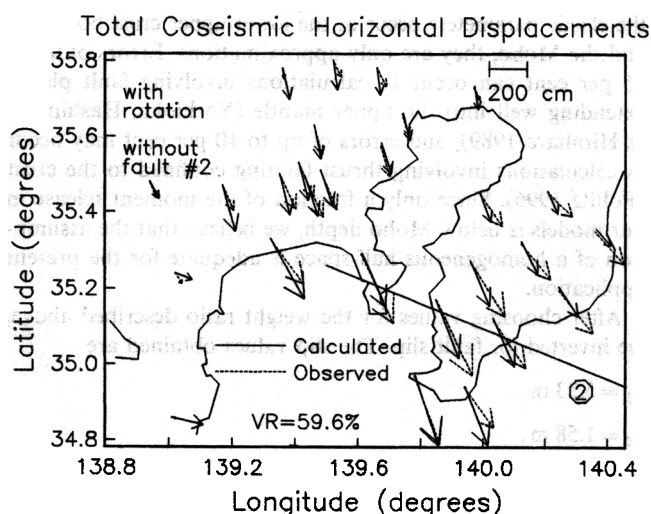


Figure 10. Rotated coseismic horizontal displacements calculated after inverting for fault slip with fault no. 2 slip fixed at zero. The 6 per cent poorer variance reduction (compared with Fig. 9) is clearly due to smaller southeast displacements of points on the Boso peninsula north of fault no. 2, the trace of which is also plotted.

this constructed data set for fault slip. To obtain estimates of the errors in slip due to errors in the horizontal data, we therefore follow a simple data perturbation scheme previously applied by Pollitz & Sacks (1996) to a geodetic inversion in Iceland. In one realization, a random data vector with zero mean and a variance of 10 cm (more precisely, 7.07 cm in both horizontal coordinate directions) is added to the observed data vector consisting of the 23 horizontal displacement vectors. This perturbed horizontal data set is, together with the vertical data set, then inverted for fault slip in the same manner as the actual data. For simplicity, errors in the vertical data are ignored. This process is repeated a large number of times to yield an estimate of the probability distribution functions for

slip and rake, or

$$f(\text{SLIP}) = \frac{dP(\text{SLIP})}{d\text{SLIP}}$$

$$f(\text{RAKE}) = \frac{dP(\text{RAKE})}{d\text{RAKE}}$$

where $P(\text{SLIP})$ and $P(\text{RAKE})$ are the probabilities that the true slip or rake is less than or equal to SLIP or RAKE , respectively. The results of this process using the various fault segments are shown in Fig. 11. It is clear that the slip estimates for all of the faults involved in the 1923 rupture are obtained with standard deviations of the order of 0.1–0.2 m, and the dip-slip component of the SE thrust is also well constrained. In particular, the slip of the Boso transform fault is a robust feature and is not an artefact of errors in the data.

4 SEQUENCE OF RUPTURE

Based on the spatial and temporal distribution of the main shock and aftershocks, as well as the revised fault geometry presented here, we propose a rupture sequence for the principal faults involved in the 1923 earthquake. Kanamori (1971) obtained an epicentre location at 35.4°N , 139.2°E for the main shock at the northeast extremity of fault no. 1. Although no seismic waveform directionality constraints are available to constrain the direction of rupture, most regions of intense crustal deformation are southeast of the main shock. In addition, the sequence of first-day aftershocks shows increasing distance from station Gifu (which is situated to the northwest of the area) (Fig. 2), implying propagation of seismic moment release towards the southeast.

The interpretation most consistent with the available information is that seismic rupture began at the northeast extremity of fault no. 1 and continued into fault no. 3, rupturing that segment partially or completely. In terms of Takemura's chronology (Fig. 2), we interpret the main shock and two other large events which also occurred around 12:00 on the

first day as representing the seismic rupture of fault no. 1 and the northwestern part of fault no. 3. Several seismic events beginning at about 12:40 on the first day (Fig. 2) are located ≥ 275 km from Gifu; that is, as far east as the Boso peninsula. We interpret this group of events as representing relatively slow seismic rupture of the southeastern and/or deeper part of fault no. 3. The horizontal slip releases obtained on fault no. 1 and fault no. 3 in the first hours of the sequence are, from the previous section, 5.5 and 3.4 m, respectively. Assuming loading of horizontal stresses distributed along the combined Sagami trough, Boso transform fault, and their southeast extensions, it follows that a deficit in horizontal slip existed along the plate boundary southeast of the Miura peninsula.

The second day of aftershocks again shows a progressive increase in distance from station Gifu with time. We interpret this as a process of gradual rupture of fault no. 2 towards the southeast. Although no fault-plane solutions are available for the two largest aftershocks of magnitude 7.3 and 7.5 (Takemura 1994), we believe that these are associated with seismic rupture of the Boso transform fault on the second day. The largest aftershock exhibits an extremely low ratio of the vertical to horizontal maximum amplitudes at 1 and 5 s periods, respectively (Takemura 1994). Takemura interpreted this as indicating a slow rupture process. Given the large seismic magnitude of the event, however, we believe that Takemura's interpretation is difficult to maintain, and it appears more likely that the low ratio is due to preferential excitement of the horizontal components by pure right-lateral slip along fault no. 2. At a 5 s period, the maximum amplitude on the horizontal components would be generated primarily by the surface waves, and an impulsive magnitude 7.5 event (rise time less than 5 s) could be generated by 1.6 m of slip along a 100–150 km long rupture on fault no. 2 (Kanamori & Anderson 1975).

The proposed sequence is compelling for several reasons. First, it may explain the large discrepancy between the seismic and geodetic moments. As pointed out by Kanamori (1973), the geodetic moment required to explain the levelling data is

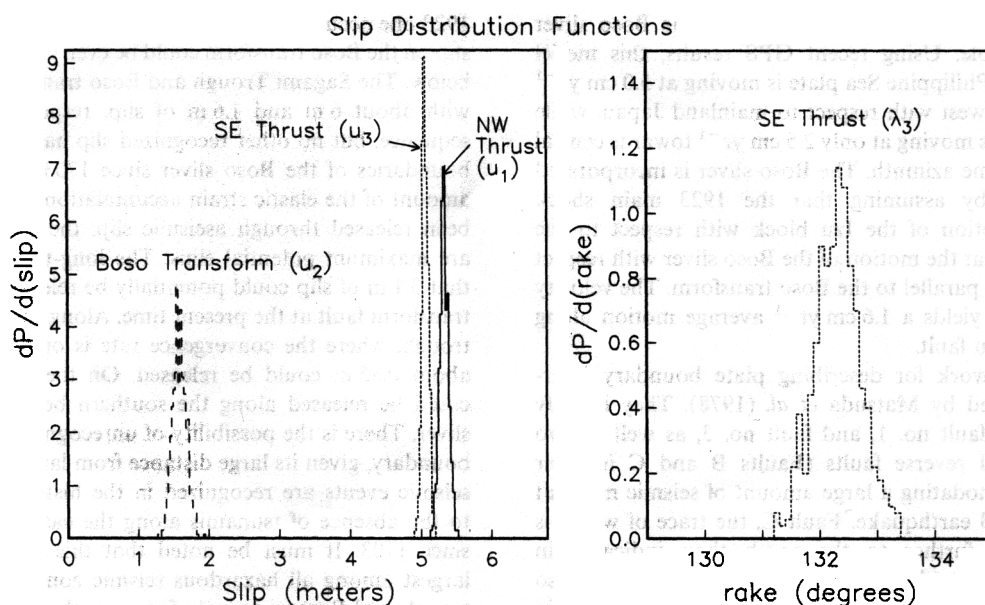


Figure 11. Probability density functions for slips u_1 , u_2 , u_3 and rake λ_3 obtained from inversion of horizontal and vertical data, using 500 realizations of a random data perturbation. The area under each curve equals unity.

about three times larger than the seismic moment detected by propagating seismic waves. If seismic slip associated with the main shock were confined to fault no. 1, this would resolve the discrepancy and remain consistent with the fault-plane solution (Fig. 1). The proposed model is also kinematically self-consistent—the horizontal component of slip is neatly partitioned between fault no. 3 and fault no. 2 southeast of the Miura peninsula. The data are not sufficient to constrain the magnitude of slip along the southeastern portion of the Boso transform fault. It would be appealing on kinematic grounds to postulate that it ruptured with about 3 m of slip southeast of the point where fault no. 3 slip terminates, and such slip values would be expected (Kanamori & Anderson 1975), given the magnitude of the largest aftershock.

These interpretations could be strengthened if fault-plane solutions were available for the largest aftershocks or if clear surface evidence existed verifying right-lateral slip of the Boso transform fault in the 1923 earthquake. There are fractures on the Miura peninsula which originated during the 1923 sequence (Yamasaki 1925; Kaine 1967), but these and other surface traces that exist on the Miura and Boso peninsulas actually yield predominantly minor dip-slip motion (Kaneko 1969). Nevertheless, right-lateral fault motions are documented on the Miura peninsula (Kaneko 1969; Research Group for Active Faults of Japan 1991), and regional kinematic considerations imply a major role for the Boso transform fault in the long term, making its participation in the 1923 earthquake more plausible (Part I).

5 GEOLOGICAL IMPLICATIONS

We shall assume here that the large-scale interactions of the Philippine Sea plate with the Japanese lithosphere around the Sagami trough are adequately described by one velocity vector, with modifications which allow for the interactions with the Boso sliver and which recognize the locally strong elastic effects near the Izu peninsula. The justification of these assumptions is discussed in greater detail in Part I.

Part I presents a new synthesis of the kinematic relationships centred around the Sagami trough in which the Boso sliver plays a central role. Using recent GPS results, this model proposes that the Philippine Sea plate is moving at 5.0 cm yr^{-1} towards the northwest with respect to mainland Japan, while the Izu peninsula is moving at only 2.5 cm yr^{-1} towards central Japan with the same azimuth. The Boso sliver is incorporated into the model by assuming that the 1923 main shock represents the motion of the Izu block with respect to the Boso sliver, and that the motion of the Boso sliver with respect to central Japan is parallel to the Boso transform. The velocity triangle in Part I yields a 1.6 cm yr^{-1} average motion along the Boso transform fault.

A useful framework for describing plate boundary interactions is presented by Matsuda *et al.* (1978). They identify the equivalent of fault no. 1, and fault no. 3, as well as two further oceanward reverse faults (Faults B and C in their Fig. 8), as accommodating a large amount of seismic moment release in the 1703 earthquake. Fault C, the trace of which is probably located further to the south than indicated in Matsuda *et al.*'s figure (i.e., at the southern end of the Boso sliver), probably did not rupture with significant reverse slip in 1923, based on the lack of a tsunami on the east coast of the Boso peninsula. Matsuda *et al.* (1978) argue that the

dominant contributor to the long-term secular uplift of the Boso peninsula is actually their Fault B. The long-term uplift rate of the southern Boso peninsula based on Holocene terraces is about 0.4 cm yr^{-1} (Matsuda *et al.* 1978). In order to couple this with Philippine Sea–Boso sliver kinematics, we modified their Fault B to lie further from land than they had proposed—shifting it slightly southeastwards to a nearby bend in the southern boundary of the Boso sliver (Fig. 1)—and assigned it a dip of 45° . A simple elastic calculation shows that about 2 cm yr^{-1} convergence on this seaward thrust is necessary to account for the southern Boso uplift rate. A shallower dip would revise this convergence rate upwards, but it seems clear that the Philippine Sea–Boso sliver convergence rate must be considerably less than the 5 cm yr^{-1} Philippine Sea–central Japan convergence rate. This supports the hypothesized motion of the Boso sliver, which implies a Philippine Sea–Boso sliver motion of 3.5 cm yr^{-1} (Part I). We therefore propose that about $1\text{--}2 \text{ cm yr}^{-1}$ of relative plate motion is accommodated by right-lateral slip along the Boso transform fault. This estimate is consistent with geological estimates derived from the reconstruction of the Boso continental margin (Part I). Although there are no observations to test whether or not this fault ruptured in 1703, the surface geology of the Miura and Boso peninsulas yields evidence of recent right-lateral movement (Yamasaki 1925; Watanabe 1926; Kaneko 1972; Research Group of Active Faults of Japan 1991; Part I).

The kinematic model described above enables us to estimate the elastic strain which could potentially be released in future earthquakes along the boundaries of the Boso sliver. Referring to Fig. 12, we shall assume that the stored strain along these boundaries was reduced effectively to zero immediately after the 1703 earthquake. This assumption is rendered plausible if one accepts the preceding interpretations of Matsuda *et al.*'s fault planes B and C—that is, the 1703 earthquake probably ruptured the entire southern boundary of the Boso sliver in addition to Sagami Bay. On the other hand, there are few or no observations available to test whether or not the 1703 sequence included rupture of the Boso transform, and it is possible that the rupture on the Boso transform preceding the 1923 one occurred before 1703. If this is true, then the potential slip on the Boso transform could be even greater than estimated below. The Sagami Trough and Boso transform fault ruptured with about 6 m and 1.6 m of slip, respectively, in the 1923 sequence, but no other recognized slip has occurred along the boundaries of the Boso sliver since 1703. Since an unknown amount of the elastic strain accumulation may have otherwise been released through aseismic slip, the estimates we derive are maximum potential slips. The long-term slip rates imply that 3.1 m of slip could potentially be released along the Boso transform fault at the present time. Along the northern Sagami trough, where the convergence rate is only 1.2 cm yr^{-1} , only about 0.85 m could be released. On the other hand, 10.5 m could be released along the southern boundary of the Boso sliver. There is the possibility of unrecognized past slip on this boundary, given its large distance from land, but no significant seismic events are recognized in the historical catalogue due to the absence of tsunamis along the eastern Boso peninsula since 1703. It must be noted that this potential slip is the largest among all hazardous seismic zones along the Nankai trough and Sagami trough; for example, we can consider the slip accumulated along the eastern Nankai trough, which last ruptured with a great earthquake in 1854 (Ishibashi 1981).

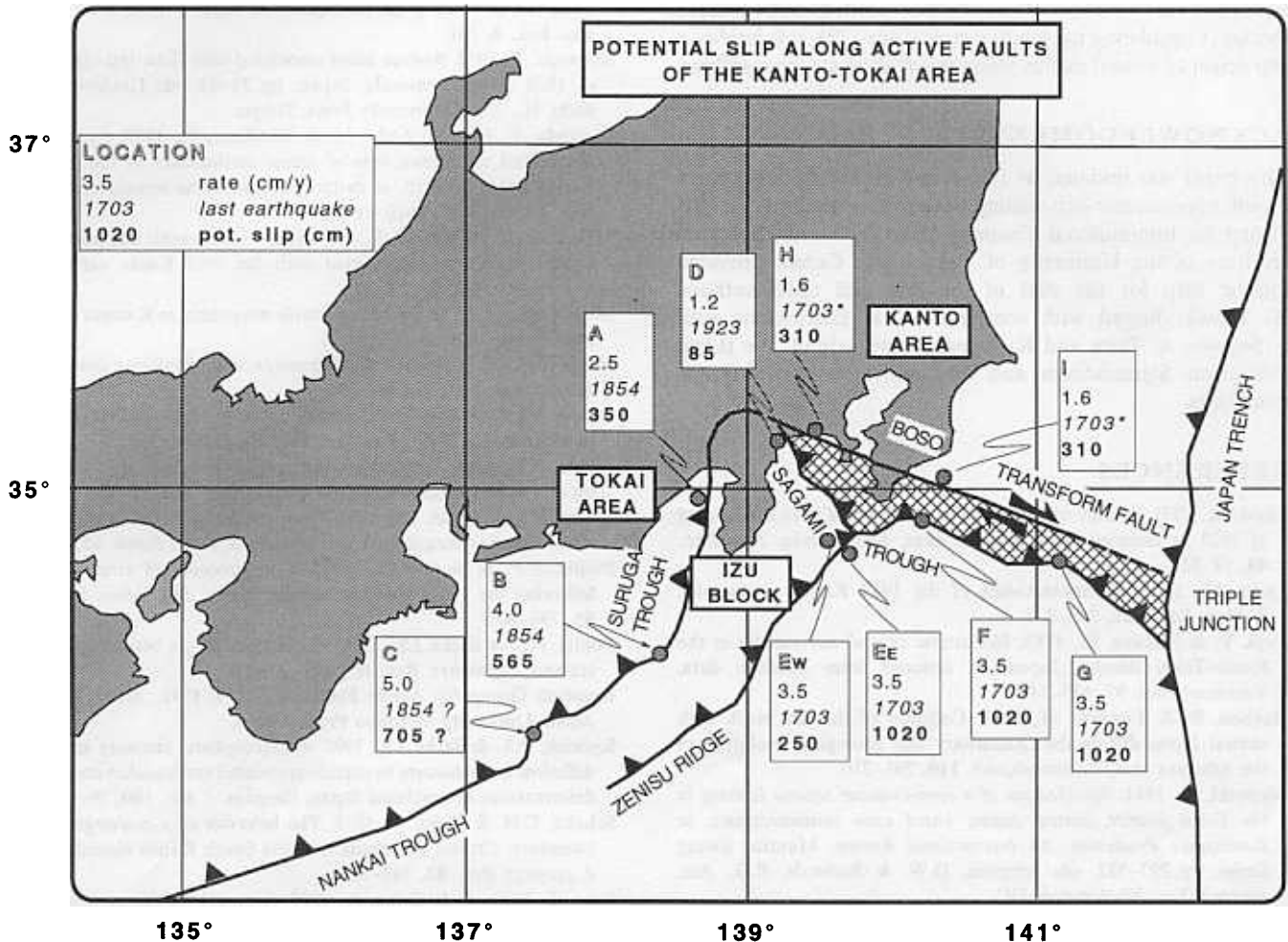


Figure 12. Potential slip release estimates along the faults bordering the Boso sliver and the Suruga trough and Nankai trough. It is assumed that stored strain was effectively reduced to zero immediately after the 1703 earthquake (around the Boso sliver) or the 1854 earthquake (Suruga trough and eastern Nankai trough). The potential slip release at the present time is simply the product of the indicated long-term slip rate and the number of years since the last major rupture.

The varying length of the subducted slab beneath Tokai district implies that the subduction rate beneath the Suruga trough is about one-half that in the western Nankai trough. This agrees with the increase in intensity of shortening of the Izu Peninsula towards the northeast. Taking 5 cm yr^{-1} for the convergence rate between the Philippine Sea plate and central Honshu, it follows that the potential slip release rises from about 3.5 m in the Suruga trough to 7 m at the western end of the seismic gap. These estimates are comparable with the potential slip release estimated by Pollitz & Sacks (1995), who used a lower convergence rate in the eastern Nankai trough but a slightly higher convergence rate in the Suruga trough.

6 CONCLUSIONS

We have taken a fresh look at the rupture process of the 1923 Kanto earthquake, motivated by on-land and marine evidence for a major recently active right-lateral transform fault (Boso transform fault) cutting through the Miura and Boso peninsulas and extending about 150 km out to sea. We have taken advantage of the results of earlier studies which explored the possible fault geometries necessary to explain the levelling

or triangulation data, and built on their models to integrate these and more recent constraints. The results show, as in earlier studies, that the Sagami trough accommodated several metres of combined right-lateral strike-slip and dip-slip motion in the 1923 sequence. In addition, the Boso transform fault slipped by about 1.6 m in a right-lateral sense. We postulate that the outstanding discrepancy between the seismic and geodetic moments for the main shock is explained by aseismic slip along the southern Sagami trough distributed throughout the first day following the main shock, and that the fault-plane solution (originally obtained by Kanamori) constrains only the seismic component of the main shock (involving the northern Sagami trough). Although kinematic constraints were not included in our inversions, the results display a partitioning of horizontal slip release between the Sagami trough and the Boso transform fault. The horizontal slip difference between the northern and southern Sagami trough in the 1923 earthquake was transferred to the adjacent Boso transform fault, which probably ruptured in conjunction with the large aftershocks on the second day following the main shock. Finally, plate kinematics and the long-term uplift history of the Boso peninsula suggest that the Boso transform fault accommodates

about 1–2 cm yr⁻¹ of the Philippine Sea–north Honshu relative motion. Considering the loading cycle since 1703, this implies a slip deficit of several metres along this fault at the present time.

ACKNOWLEDGMENTS

This paper was initiated by the second author during a three month appointment as a visiting Professor in the newly created Center for International Cooperation in the Ocean Research Institute of the University of Tokyo. The Center provided logistic help for the visit of the first and third authors. K. Tamaki helped with computer work. Discussions with J. Segawa, A. Taira and K. Tamaki were helpful. We thank Freysteinn Sigmundsson and an anonymous reviewer for comments.

REFERENCES

- Ando, M., 1971. A fault-origin model of the Great Kanto earthquake of 1923 as deduced from geodetic data, *Bull. Earthq. Res. Inst.*, **49**, 19–32.
- Ando, M., 1974. Seismo-tectonics of the 1923 Kanto earthquake, *J. Phys. Earth*, **22**, 263–277.
- Fujii, Y. & Nakane, K., 1983. Horizontal crustal movements in the Kanto-Tokai district, Japan, as deduced from geodetic data, *Tectonophysics*, **97**, 115–140.
- Huchon, P. & Kitazato, H., 1984. Collision of the Izu block with central Japan during the Quaternary and geological evolution of the Ashigara area, *Tectonophysics*, **110**, 201–210.
- Ishibashi, K., 1981. Specification of a soon-to-occur seismic faulting in the Tokai district, central Japan, based upon seismotectonics, in *Earthquake Prediction: An International Review*, Maurice Ewing Series, pp. 297–332, eds Simpson, D.W. & Richards, P.G., Am. geophys. Un., Washington, DC.
- Ishida, M., 1992. Geometry and relative motion of the Philippine Sea plate beneath the Kanto-Tokai district, Japan, *J. geophys. Res.*, **97**, 489–513.
- Kaine, Y., 1967. Activity of the Shitaura Fault during the Great Kanto earthquake, *Miura Archives (Keihin Express)*, no. 3, 115–120.
- Kanamori, H., 1971. Faulting of the Great Kanto earthquake of 1923 as revealed by seismological data, *Bull. Earthq. Res. Inst.*, **49**, 13–18.
- Kanamori, H., 1973. Mode of strain release associated with major earthquakes in Japan, *Ann. Rev. Earth planet Sci.*, **1**, 213–239.
- Kanamori, H. & Anderson, D.L., 1975. Theoretical basis of some empirical relations in seismology, *Bull. seism. Soc. Am.*, **65**, 1073–1095.
- Kanamori, H. & Miyamura, S., 1970. Seismometrical re-evaluation of the Great Kanto earthquake of September 1, 1923, *Bull. Earthq. Res. Inst.*, **48**, 115–125.
- Kaneko, S., 1969. Right-lateral faulting in Miura Peninsula, south of Tokyo, Japan, *J. geol. Soc. Japan*, **4**, 199–208.
- Kaneko, S., 1971. Neotectonics of Oiso Hills and contiguous districts in south Kanto, Japan, *J. geol. Soc. Japan*, **77**, 345–358.
- Kaneko, S., 1972. Some remarks on the strike-slip faulting in Miura Peninsula and Sagami Bay area, south Kanto, Japan, *J. geol. Soc. Japan*, **78**, 203–212.
- Lallemand, S., Le Pichon, X., Thoué, F. & Henry, P., 1996. Shear partitioning near the central Japan triple junction: the 1923 great Kanto earthquake revisited—I, *Geophys. J. Int.*, **126**, 871–881 (Part I; this issue).
- Land Survey Department, 1928. Provisory map showing the horizontal displacements of the primary triangulation points in Kanto districts, observed after the great earthquake of Sept. 1, 1923, *Bull. Earthq. Res. Inst.*, **4**, 231.
- Matsuda, T., 1972. Surface faults associated with Kita-Izu earthquake of 1930 in Izu Peninsula, Japan, pp. 73–93, eds Hoshino, M. & Aoki, H., Tokai University Press, Tokyo.
- Matsuda, T., Ota, Y., Ando, M. & Yonekura, N., 1978. Fault mechanism and recurrence time of major earthquakes in the southern Kanto district, Japan, as deduced from coastal terrace data, *Geol. Soc. Am. Bull.*, **89**, 1610–1618.
- Matsu'ura, M. & Iwasaki, T., 1983. Study on coseismic and postseismic crustal movements associated with the 1923 Kanto earthquake, *Tectonophysics*, **97**, 201–215.
- Miyabe, N., 1931. On the vertical earth movement in Kwanto districts, *Bull. Earthq. Res. Inst.*, **9**, 1–21.
- Muto, K., 1932. A study of displacements of triangulation points, *Bull. Earthq. Res. Inst.*, **10**, 394–391.
- Okada, Y., 1985. Surface deformation due to shear and tensile faults in a half-space, *Bull. seism. Soc. Am.*, **75**, 1135–1154.
- Pollitz, F.F., 1996. Coseismic deformation from earthquake faulting on a layered spherical earth, *Geophys. J. Int.*, **125**, 1–14.
- Pollitz, F.F. & Sacks, I.S., 1994. Fault model of the Nobi earthquake from historic triangulation and leveling, *J. Phys. Earth*, **42**, 1–43.
- Pollitz, F.F. & Sacks, I.S., 1995. Consequences of stress changes following the 1891 Nobi earthquake, Japan, *Bull. seism. Soc. Am.*, **85**, 796–807.
- Pollitz, F.F. & Sacks, I.S., 1996. Viscosity structure beneath northeast Iceland, *J. geophys. Res.*, in press.
- Research Group for Active Faults of Japan, 1991. *Active Faults in Japan*, University of Tokyo Press, Tokyo.
- Rydelek, P.A. & Sacks, I.S., 1990. Asthenospheric viscosity and stress diffusion: a mechanism to explain correlated earthquakes and surface deformations in northeast Japan, *Geophys. J. Int.*, **100**, 39–58.
- Scholtz, C.H. & Kato, T., 1978. The behavior of a convergent plate boundary: Crustal deformation in the South Kanto district, Japan, *J. geophys. Res.*, **83**, 783–797.
- Seno, T., Stein, S. & Gripp, A., 1993. A model for the motion of the Philippine Sea plate consistent with NUVEL-1 and geological data, *J. geophys. Res.*, **98**, 17 941–17 948.
- Sugimura, A., 1972. Plate boundaries in and near Japan, *Kagaku*, **42**, 192–202.
- Sugimura, A. & Naruse, Y., 1954. Changes in sea level, seismic upheaval, and coastal terraces in southern Kanto region, Japan (I) *J. Geol. Geogr.*, **24**, 101–113.
- Tabei, T., 1989. Crustal movements in the inner zone of southwest Japan associated with stress relaxation after major earthquakes, *J. Phys. Earth*, **37**, 101–131.
- Takemura, M., 1994. Aftershock activities of two days after the 1923 Kanto Earthquake (M = 7.9) inferred from seismograms at Gifu observatory, *Zishin*, **46**, 439–445 (in Japanese).
- Thatcher, W., 1984. The earthquake deformation cycle at the Nankai Trough, southwest Japan, *J. geophys. Res.*, **89**, 3087–3101.
- Thatcher, W., Matsuda, T., Kato, T. & Rundle, J.B., 1980. Lithospheric loading by the 1896 Riku-earthquake, northern Japan: Implications for plate flexure and asthenospheric rheology, *J. geophys. Res.*, **85**, 6429–6435.
- Watanabe, K., 1926. The dislocation of Kitashitauramura, Miura Peninsula, *J. Geogr.*, **35**, 592–596.
- Yamasaki, N., 1925. Physiographical investigation of the Great earthquake of S.E. Japan, *Rep. Imperial Earthq. Investigation Committee*, **100 B**, 11–35.
- Yoshioka, S., Hashimoto, M. & Hirahara, K., 1989. Displacement fields due to the 1946 Nankaido earthquake in a laterally inhomogeneous structure with the subducting Philippine Sea plate—a three-dimensional finite element approach, *Tectonophysics*, **159**, 121–136.